MULTITEMPERATURE ANALYSIS OF SOLAR X-RAY LINE EMISSION

J. SYLWESTER*, J. SCHRIJVER, and R. MEWE
The Astronomical Institute, Space Research Laboratory, Utrecht, The Netherlands

(Received 9 November, 1979; in revised form 18 February, 1980)

Abstract. In this paper we propose and test a new method of multitemperature analysis of solar X-ray spectra. The method, which is based on a technique developed by Withbroe (1975), is designed to be used in the interpretation of spectra, to be measured by the X-Ray Polychromator on the Solar Maximum Mission. Various tests of the method on simulated temperature models establish its usefulness, generality, and stability. The possibilities of deriving the relative element abundances are analysed. The results of the present paper extend the possibility of the multitemperature analysis of X-ray spectra as compared with the results of Craig and Brown (1976a, b) and Craig (1977).

1. Introduction

The determination of the temperature structure of a hot ($T \gtrsim 10^6$ K), optically thin plasma is one of the main problems in astrophysical plasma diagnostics. Many attempts have been made to develop the best method for the multitemperature analysis of a solar active region plasma. In several early papers the authors have assumed a constant temperature all over the emitting region. With this assumption, the flux ratios measured in suitable lines or wavelength bands were used to derive two plasma parameters: temperature T and emission measure ε (Kahler *et al.*, 1970; Landini *et al.*, 1972). However, the temperature derived from different flux ratios yields values from 1.5 to at least 30×10^6 K during solar flares, so it seems natural to use a multitemperature model of the emitting plasma in the analysis of solar X-ray data covering the extended wavelength region 1–25 Å.

Batstone *et al.* (1970), Chambe (1971), Walker (1972), Meekins (1973), Jakimiec *et al.* (1974), Walker *et al.* (1974a, b, c), Phillips (1975), Parkinson (1975a), have analyzed the X-ray line emission of non-flaring solar active regions in terms of a multitemperature model. Analysis of solar X-ray flare data was performed by Horan (1971), Herring and Craig (1973), Dere *et al.* (1974), Horan *et al.* (1974), Craig (1975), Sylwester (1980), Landini and Monsignori Fossi (1979).

Craig and Brown (1976a, b) have strongly criticized the multitemperature analysis of X-ray spectra and point out 'fundamental limitations' of such a type of analysis. But they use a mathematical method of solution that is inappropriate for this problem, as it does not exclude *a priori* negative values of the emission measure. In the context of the present paper, this point seems to be the main cause of their very critical statements.

* On leave from Polish Academy of Sciences, Space Research Center, Wrocław, Kopernika 11, Poland.

The aim of our paper is to propose and to test a new method of multitemperature analysis of X-ray spectra, based on the paper by Withbroe (1975). The method is designed to be used in the interpretation of spectra, to be measured by the X-Ray Polychromator (XRP) Flat Crystal Spectrometer, part of the Solar Maximum Mission (SMM) (Acton *et al.*, 1980). The paper shows that the multitemperature analysis of solar X-ray line emission is valuable and useful. In the following sections we redefine the differential emission measure (DEM), present the method used, perform various tests, indicate the possibility of an *a posteriori* search for instrument calibration errors, and point out how to determine relative element abundances. Everywhere in the paper we use the assumption of quasistationarity of the emitting plasma, which means that we assume that the relaxation time of the ionization equilibrium in the emitting plasma is shorter than the characteristic time of the temperature variations. The analysis of a nonequilibrium plasma is presented elsewhere (cf. Sylwester *et al.*, 1980).

2. Differential Emission Measure

The concept of a differential emission measure (DEM) was considered by Jefferies *et al.* (1972), Walker *et al.* (1974a), Phillips (1975), Sylwester (1977). The most suitable definition of DEM seems that given by Equation (9) in Craig and Brown (1976b). But this definition, which involves an inverse temperature gradient, cannot be used in the case of a partly isothermal region. This is the reason why we shall introduce here an alternative, physically simple definition of DEM, based on a concept of Jefferies *et al.* (1972).

The X-ray spectrum for an optically thin thermal source may be written

$$F(\lambda) = \iiint_V \mathscr{F}(\lambda, T(\mathbf{r})) N_e^2(\mathbf{r})\, \mathrm{d}^3\mathbf{r}\,, \tag{1}$$

where $N_e(\mathbf{r})$ and $T(\mathbf{r})$ are the electron density and temperature at position $\mathbf{r}$ in the source of volume V, λ is the wavelength of the emitted radiation, and $\mathscr{F}(\lambda, T)$ denotes the theoretical spectral distribution function for an isothermal volume element of temperature T.

Let us assume V to be the volume inside a spatial resolution element of the spectrometer used. The emitting plasma is assumed to be optically thin, so any simple geometrical rearrangement of the material inside V will produce the same photon emission. To characterize the volume structure of the plasma we can introduce a bivariate, volume vs temperature and electron density, distribution function $\mathscr{V}(T, N_e)$. The normalisation condition for this distribution will be

$$\int_{T=0}^{\infty} \int_{N_e=0}^{\infty} \mathscr{V}(T, N_e)\, \mathrm{d}T\, \mathrm{d}N_e = V = \iiint \mathrm{d}^3\mathbf{r}\,. \tag{2}$$

Here $\mathcal{V}(T, N_e)\,\mathrm{d}T\,\mathrm{d}N_e$ describes the volume element inside V which is occupied by matter with temperature between T and $T+\mathrm{d}T$ and density between N_e and $N_e+\mathrm{d}N_e$. $\mathcal{V}(T, N_e)$ involves all elementary volumes inside V characterized by the same temperature T and density N_e.

Now we introduce the electron distribution function $\mu(T, N_e)$ by means of the expression

$$N_e\,\mathrm{d}V = \mathrm{d}N(T, N_e) = N\mu(T, N_e)\,\mathrm{d}N_e\,\mathrm{d}T, \tag{3}$$

with $\mathrm{d}N$ the total *number* of electrons inside the resolution element sampled by the observation, that are present in the interval $(\mathrm{d}T, \mathrm{d}N_e)$. Integrating Equation (3) over N_e we obtain the number of electrons $N(T)\,\mathrm{d}T$ being inside the temperature interval $\mathrm{d}T$:

$$N(T)\,\mathrm{d}T = N\Phi(T\,\mathrm{d}T)\,. \tag{4}$$

Here

$$\Phi(T) = \int_{N_e=0}^{\infty} \mu(T, N_e)\,\mathrm{d}N_e$$

is the temperature distribution function for electrons inside V.

Using Equations (1), (2), (3) we obtain

$$\begin{aligned} F(\lambda) &= \int_{T=0}^{\infty}\int_{N_e=0}^{\infty} \mathcal{F}(\lambda, T)NN_e\mu(T, N_e)\,\mathrm{d}N_e\,\mathrm{d}T \\ &= \int_{T=0}^{\infty} \mathcal{F}(\lambda, T)\left[N\int_{N_e=0}^{\infty} N_e\mu(T, N_e)\,\mathrm{d}N_e\right]\mathrm{d}T. \end{aligned} \tag{5}$$

Let us call the integral

$$\phi(T) = N\int_{N_e=0}^{\infty} N_e\mu(T, N_e)\,\mathrm{d}N_e \tag{6}$$

the differential emission measure at temperature T. Using the mean electron density $\bar{N}_e(T)$ defined as

$$\bar{N}_e(T) = \frac{\int_{N_e=0}^{\infty} N_e\mu(T, N_e)\,\mathrm{d}N_e}{\int_{N_e=0}^{\infty} \mu(T, N_e)\,\mathrm{d}N_e}, \tag{7}$$

Equation (6) becomes

$$\phi(T) = N\bar{N}_e(T)\Phi(T)\,. \tag{8}$$

So, the DEM at a given temperature T is a product of the temperature distribution

function for N electrons inside V and their mean density at this temperature. Equation (8) can be particularly useful when attempts are made to derive DEM distributions from theoretical considerations giving the relation between $\bar{N}_e(T)$ and $\Phi(T)$. From Equation (8) it clearly follows that $\phi(T)$ is a temperature distribution function.

Rewriting Equation (5) with the use of Equation (8) for the case of an X-ray emission line 'i' we find

$$F_i = A_i \int_{T=0}^{\infty} f_i(T)\phi(T)\,\mathrm{d}T. \tag{9}$$

We have assumed here that the abundance A_i (of the element forming line i) relative to hydrogen is constant inside volume V; $f_i(T)$ is the emission function in the line (the flux in the line at a distance of 1 AU emitted by a plasma of unit emission measure at temperature T, with unit abundance). Values of $f_i(T)$ can be calculated theoretically (see later).

3. Method of DEM Distribution Calculations

The calculation of a model (hereafter the term 'model' denotes the DEM distribution) of the emitting region is the main aim of many XUV and X-ray spectroscopy experiments (see Walker, 1972; Jordan, 1975; Parkinson, 1975b; and Walker, 1975). The data often used for this purpose are absolute fluxes in several strong X-ray lines. Because of the different temperature sensitivity (different corresponding $f_i(T)$ functions) of the lines used, the thermal structure of the emitting regions is reflected by the relative fluxes of the measured lines. In the process of model determination we try to find that temperature model $\phi(T)$ of the emitting region, which gives agreement between the calculated and the measured fluxes in the lines.

Mathematically, the problem can be posed in the following manner: we have measured fluxes F_i, $i = 1 \ldots k$, for which the emission functions and abundances are known, and we try to find the model function $\phi(T)$ (always non-negative) by solving the system of Equations (9) with $i = 1 \ldots k$.

Some different methods have been proposed to solve this system: the quadrature method in which the integral is replaced by some quadrature approximation (Batstone *et al.*, 1971; Parkinson, 1975a) after which a system of linear equations is solved using appropriate techniques; the method of parametric functions, in which $\phi(T)$ is represented in the form of an assumed parametric expression (Chambe, 1971; Walker *et al.*, 1974a; Phillips, 1975), and after integration, the parameter values are found usually by means of a best fit procedure. An extensive mathematical analysis of the quadrature method of solution for Equation (9) can be found in Rust and Burrus (1972).

The reality and inner consistency of model calculations are discussed often in terms of the parameter χ^2 given as

$$\chi^2 = \sum_{i=1}^{k} \frac{(F_i - F_{ic})^2}{\sigma_i^2}, \tag{10}$$

where F_{ic} is the line flux calculated from model $\phi(T)$ using Equation (9). The error σ_i should be interpreted as an error consisting of the uncertainties in the measurements, in the abundances A_i, and in the function $f_i(T)$. In the following calculations we have assumed, for simplicity, the last two uncertainties to be negligible.

A χ^2 value near the expected value indicates that the calculated model is in agreement with the measured line fluxes. The interpretation of χ^2 values in the case of a parametric estimation can be found in Lampton *et al.* (1976).

The expected high resolution and calibration accuracy of the planned XRP experiment (Rapley, 1977) may create a situation, where a significant difference exists between the accuracy of the measurements and the level of sophistication of the methods for data analysis. We have performed a critical search for the accuracy and the possibilities of existing methods of line flux analysis and we have found that most of the proposed methods are not sufficiently general and not able to match different expected models of active regions (both flaring and non-flaring). The quadrature methods are limited by the number of lines of different temperature sensitivity, while the parametric method limits the class of models which can be fitted by assuming *a priori* a general form or $\phi(T)$. Only one method, used for the analysis of the chromosphere-corona transition region (Withbroe, 1975) seems to be a good basis for the model analysis. It fulfils the condition that $\phi(T) \geq 0$ and can meet our needs in accuracy after some modifications.

The method is an iterative procedure in which the next approximation of the model, $\phi_{j+1}(T)$, is calculated from the preceding one, $\phi_j(T)$, by means of the following formula:

$$\phi_{j+1}(T) = \phi_j(T) \frac{\sum_{i=1}^{k} CF_i W_i(T)}{\sum_{i=1}^{k} W_i(T)}. \tag{11}$$

The weight functions $W_i(T)$ are chosen such that the correction factor $CF_i = F_i/F_{ic}$ improves the model most efficiently at those temperatures, where the particular line i is formed:

$$W_i(T) = f_i(T)\phi_j(T) \frac{\int_0^\infty f_i(T)\phi_j(T)\,\mathrm{d}T}{\int_0^\infty [f_i(T)\phi_j(T)]^2\,\mathrm{d}T} \left[\frac{|F_i - F_{ic}|}{\sigma_i} + 1\right]^a, \tag{12}$$

$$F_{ic} = A_i \int_0^\infty f_i(T)\phi_j(T)\,\mathrm{d}T, \tag{13}$$

where the parameter $a \geq 0$ (or < 0) for $F_i \geq$ (or $<$) F_{ic}. The last factor in parentheses,

which has been added to the weighting function used by Withbroe (1975), takes into account the errors of the flux measurements. It is defined such that when the difference between the measured and calculated fluxes of a particular line (F_i and F_{ic}, respectively) is relatively high, it significantly differs from 1, thus laying more emphasis on the correction of the model for this line. The form of this error weight was found semi-empirically. It turns out that by taking a value for the parameter a of the order of σ_i/F_i, we obtain the best convergence of the iteration procedure.

From the formulae for the iterative procedure it is clearly seen that the method gives non-negative values for $\phi(T)$ (the operations to be performed to calculate the next approximation for $\phi(T)$ do not change the sign). By this property the method fulfils the requirement that the emission measure should always be positive. In the calculations one can use a zero approximation $\phi_0(T) = \text{const.}$, which seems reasonable when no other *a priori* information exists.

An important step after the model determination is the estimation of errors in the model caused by errors in the measured line fluxes. Our intention is to find the set of models which gives an agreement between measured and calculated fluxes better or equal to the errors of measurement σ_i. This condition can be written in the form of a set of integral equations:

$$F_i \pm \sigma_i \geq A_i \int_0^\infty [\phi_c(T) \pm \psi(T)] f_i(T)\, \mathrm{d}T, \qquad i = 1 \ldots k, \tag{14}$$

where $\phi_c(T)$ denotes the best model calculated and $\psi(T)$ is the unknown error function. Equation (14) can be rewritten using Equation (9) as

$$\sigma_i^* = |F_i - F_{ic}| + \sigma_i \geq A_i \int_0^\infty \psi(T) f_i(T)\, \mathrm{d}T, \qquad i \ldots k. \tag{15}$$

The absolute value of the difference between the measured and the calculated line fluxes can thus be treated as a part of the estimated maximum error σ_i^* in the line i.

Equation (15) for the error function $\psi(T)$ has been solved analytically for the following two cases:

(1) 'Single-temperature' error case.

(2) 'Continuous' error case.

In the first case we assume that $\psi(T)$ is a delta-type function, which means physically that the calculated model $\phi_c(T)$ is everywhere a very good approximation to the real distribution, except at one temperature T_0, where deviations $\pm\psi(T_0)$ occur.

Solving Equation (15) separately for each line we obtain a set of equations for $\psi_i(T_0)$, $i = 1 \ldots k$:

$$\psi_i(T_0) = \frac{\sigma_i^*}{A_i f_i(T_0)}, \qquad i = 1 \ldots k. \tag{16}$$

For each temperature T_0 we thus have k $\psi_i(T_0)$ values, the smallest value of which gives the error:

$$\psi_M(T_0) = \min |\psi_i(T_0)|, \qquad i = 1 \ldots k. \tag{17}$$

The values $\pm \psi_M(T_0)$ define the 'maximal' perturbation which can be inserted in the model $\phi_c(T)$ at temperature T_0 without giving a disagreement between calculated and observed line fluxes greater than any of the σ_i^* errors.

In the second case we assume that the error $\psi_i(T)$ in line i is smoothly distributed over the whole temperature range of line formation ΔT_i, in the sense that each temperature interval inside ΔT_i gives the same contribution to the error, i.e.

$$\psi_i(T) f_i(T) = \text{const. inside } \Delta T_i,$$

$$\psi_i(T) f_i(T) = 0 \text{ outside.}$$

We define ΔT_i as the temperature interval where 99% of the line flux arises in the model $\phi_c(T)$.

Using Equation (15) we obtain

$$\psi_i(T) = \frac{\sigma_i^*}{A_i f_i(T) \Delta T_i}, \qquad i = i \ldots k. \tag{18}$$

Taking again

$$\psi_c(T) = \min |\psi_i(T)|, \qquad i = 1 \ldots k, \tag{19}$$

we define the limits $\phi_c(T) \pm \psi_c(T)$ for the family of continuous model solutions which result in line fluxes being in agreement with the measured fluxes better than the σ_i^* errors.

The temperature range ΔT where $|\phi_c(T)| \geq |\psi_c(T)|$ can indicate roughly the temperature interval where the model estimation is meaningful. This interval will be important for model comparison (see next section).

It should be noted that the way of error analysis presented is very simple. One can investigate this problem statistically by solving many times the system of Equations (9), after adding to the measured fluxes errors distributed normally with standard deviation σ_i. The resulting family of solutions can give information about the possible errors in the model estimation. Such an error analysis can be made for any set of measured line fluxes.

4. Tests of the Iterative Method

The simplest way to test a complicated iterative procedure for model calculations is to check the results of its application in the analysis of artificially generated models, i.e. to look how closely the calculated models agree with the ideal generated ones. The procedure for such a comparison can be as follows. Using the assumed model

$\phi_g(T)$ we can calculate the fluxes in the set of basic lines using the formula

$$F_{ig} = A_i \int_0^\infty f_i(T)\phi_g(T)\,\mathrm{d}T. \tag{20}$$

Then, these fluxes can be treated as observed ones ($F_i = F_{ig}$) and used as input data for the iterative method. As the result of the iterative calculations we obtain the model $\phi_c(T)$ which corresponds to the smallest χ^2 value occuring in the calculations. As a test of the agreement we can use the value of the following parameter:

$$\sigma = \frac{1}{\Delta T} \int_{\Delta T} \left[\frac{\phi_g(T) - \phi_c(T)}{\phi_g(T) + \phi_c(T)}\right]^2 \mathrm{d}T, \tag{21}$$

where ΔT is the temperature interval in which we compare the assumed and calculated models. This interval should be chosen in accordance to the temperature interval in which the lines are sensitive to model variation. From Equation (21) it is seen that $\sigma = 0$ when $\phi_g(T) \equiv \phi_c(T)$ and $\sigma \simeq 1$ when $\phi_g(T)/\phi_c(T)$ differs much from unity. The parameter σ is convenient for the comparison of continuous distributions, the absolute values of which change by many orders inside the comparison interval, but it is not very useful when calculated models (always continuous) are compared with assumed models of the delta-type. In such cases we shall use two parameters: T_m – the temperature of the maximum in the calculated $\phi_c(T)$ distribution and the value of the FWHM of this distribution. These two values together with ε (see later) characterize the fit of the continuous distribution to the delta-type one. As a universal test parameter we will use the ratio $\varepsilon_c/\varepsilon_g$ of calculated to assumed total emission measure. ε is defined by

$$\varepsilon = \int_{\Delta T} \phi(T)\,\mathrm{d}T. \tag{22}$$

From Craig and Brown (1976b) follows that a very important characteristic of a method is its stability. Stability in this context relates to the response of the calculated model to perturbations in the line fluxes used. If small perturbations in measured fluxes (measurement errors) induce strong variations in the solution, than the *method* (not always the problem) is unstable and can not be successfully used. The stability test can be performed by comparison of σ, or T_m and the FWHM values for perturbed models with unperturbed ones.

The inspection of usefulness, accuracy and stability of the proposed method can also be made by visual comparison of generated and calculated models. Such a comparison can give an impression of the limits of the physical interpretation of the measured fluxes.

5. Results

We have based our tests of the method on two sets of lines, which could be measured by means of the XRP spectrometer. The first set consists of 7 lines, planned to be used in the Polychromator Mapping Mode (PMM) (Rapley, 1977). These lines are denoted by an asterisk in Table I. The other, extended set involves the PMM set plus 7 other lines which are given also in Table I. All the lines used are resonance, most prominent lines arising from the H and He like ions of 7 elements: O, Ne, Mg, Si, S, Ca, and Fe. Emission functions for these lines were calculated using the collision strength approximation of Mewe *et al.* (1980a). The ionization equilibrium calculations were performed using the rate coefficients given by Mewe and Schrijver (1978) as updated by Mewe *et al.* (1980a, b). In the resonance line emission function calculations we took into account the processes of: direct excitation, cascades, radiative recombination, and dielectronic recombination.

TABLE I

The set of resonance lines used in the model analysis

Line No.	λ (Å)	Isolectr. sequence	Element	T_{max} (10^6 K)
1	1.7805	H	Fe	130
2*	1.8505	He	Fe	71
3	3.0209	H	Ca	58
4*	3.1770	He	Ca	30.5
5	4.7295	H	S	26.5
6*	5.0386	He	S	15.5
7	6.1824	H	Si	16.7
8*	6.6478	He	Si	10.5
9	8.4211	H	Mg	10.2
10*	9.1688	He	Mg	6.3
11	12.1338	H	Ne	5.9
12*	13.4481	He	Ne	4.1
13*	18.9687	H	O	3.0
14	21.6044	He	O	2.1

Theoretical wavelengths are taken from Vainshtein and Safronova (1978), and are corrected for the Lamb shift (+0.0007 Å), (cf. Korneev *et al.*, 1979). For H-doublets the mean value of λ is given. T_{max} is the temperature of maximum power emitted in the line (cf. Figure 1).

* Used in the Polychromator Mapping Mode of XRP.

We present in Figure 1 the calculated emission functions. The numbers denoting functions correspond to line numbers in Table I. The temperatures T_{max} where maximum power is emitted in the lines cover the range from 2 to $\sim 70 \times 10^6$ K. We have therefore used this temperature interval for the model calculations. The heavier lines in Figure 1 correspond to the PMM line set.

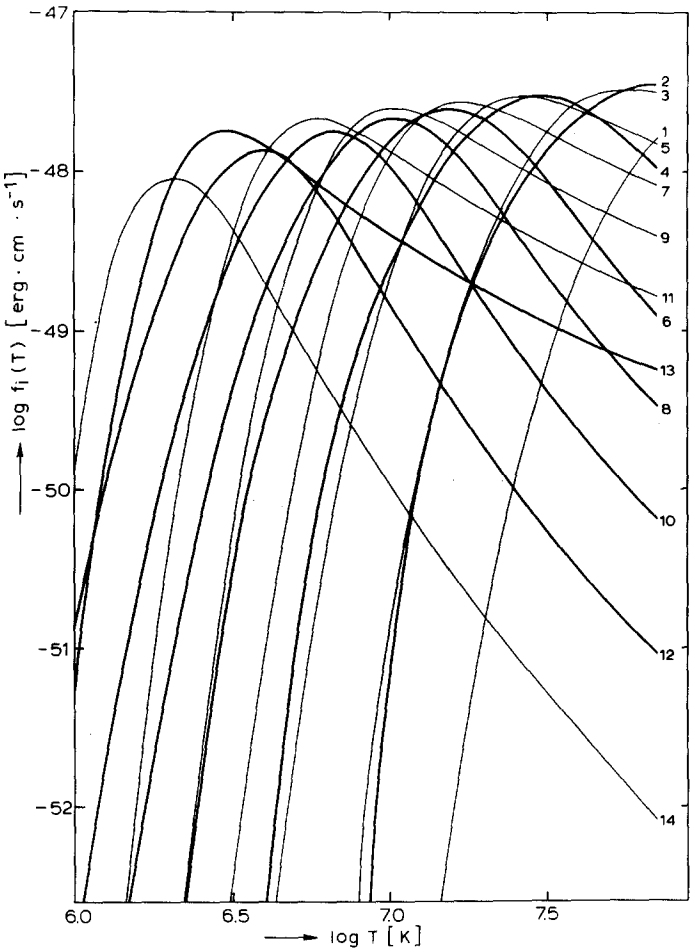

Fig. 1. Calculated emission functions for the 14 lines used in the model analysis. Number denoting curves correspond to lines in Table I (heavy curves indicate the lines of the PMM line set).

In the model calculations we have everywhere assumed a *constant* zero approximation model $\phi_0(T) = 2 \times 10^{42}\ \mathrm{cm}^{-3}\ \mathrm{K}^{-1}$. We have found that the resulting best model hardly depends on the shape of the zero approximation, as long as this approximation does not oscillate with a characteristic period shorter than 30×10^6 K, but we have found that a suitable zero approximation can save much computer time.

The use of a constant zero approximation seems to be a justified assumption when other information does not exist. Physically it means that we assume that the emission measure is equally distributed over all temperatures. The assumption of a constant emission measure implies some kind of smoothing in the solution (smooth $\mathrm{d}\phi(T)/\mathrm{d}T$). If some foreknowledge about the structure of the model is available, such information can easily be taken into account in the zero approximation.

After many test calculations we have found that in most cases it is sufficient to stop the model calculations after about 150 iteration steps, since convergence within

0.1% for the model function $\phi(T)$ is then reached. As the best calculated model $\phi(T)$ we have adopted the model corresponding to the smallest χ^2 value. In all cases considered (except in some cases for perturbed model calculations, see later) the parameter χ^2 converged until the last iteration.

First we have tested the ability of the method to fit different assumed (generated) models. The results of calculations for continuous generated models of the type $\phi_g(T) = A \times 10^{-\alpha T}$ are presented in Figures 2, 3, and 4. In Figures 5 and 6 fits to delta-type models are presented. Figures 7 and 8 deal with mixed (continuous + delta-type) models. In all these figures the heavy line corresponds to the model calculated using the PMM line set while the dashed line refers to the calculations based on the extended line set. In Figure 2 we have hatched the 'continuous' error

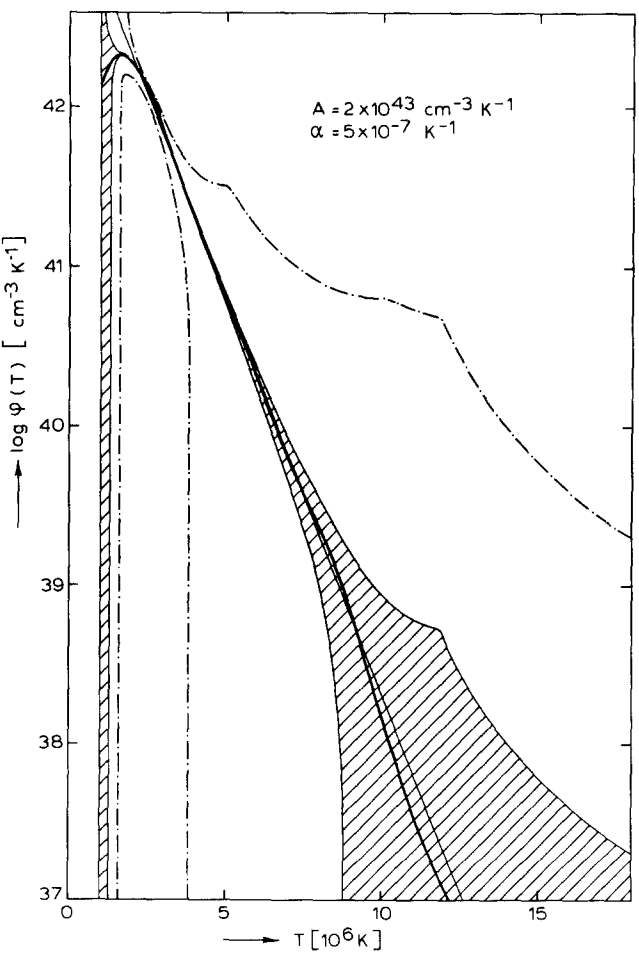

Fig. 2. Comparison of assumed (thin line) with calculated (heavy line) model. The 'continuous' error area is hatched, while dash-dot lines represent the 'single-temperature' error limits. The calculations were done for the PMM line set. For the calculation of the error see text.

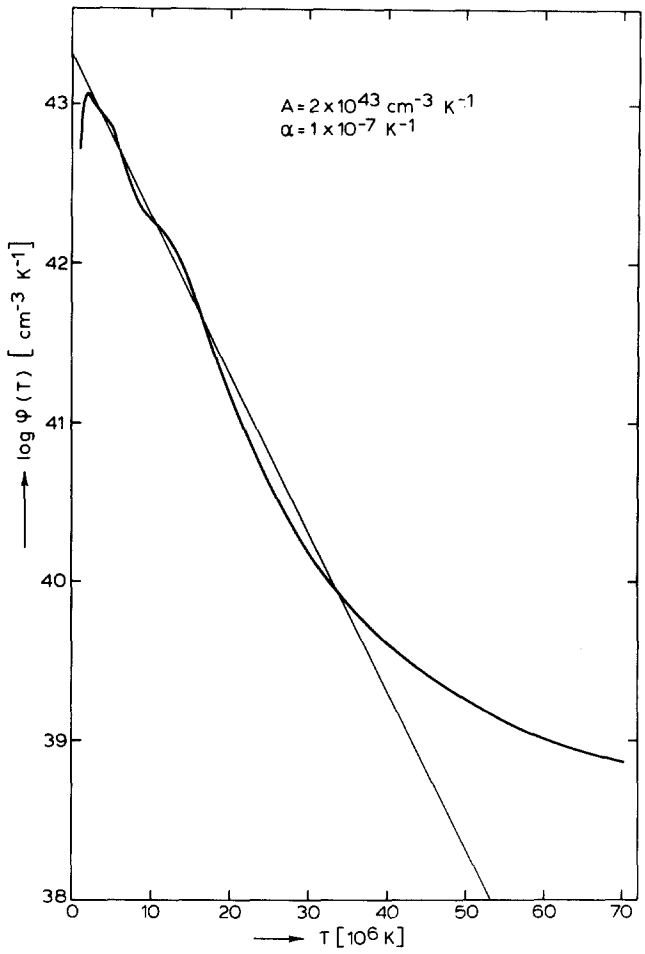

Fig. 3. Comparison of assumed (thin line) with calculated (heavy line) model. Calculations are based on the PMM set of lines.

area (every model inside this area is in agreement with the 'measured' line fluxes within the errors σ_i^* (see Equations (15), (18), and (19)). The error σ_i we have calculated by taking the square root of the number of counts in line i as measured by the FCS in a 1 s integral scan and assuming for simplicity an efficiency $\sim 0.01/\lambda_i$ ct cm^2 phot^{-1} (λ_i is wavelength of line i in Å). The limits of the single-temperature error (Equations (16) and (17)) in the model are also presented (dash-dot line). The characteristics of the model fitting for the continuous and delta-type models are given in Table II.

Comparison shows that for all continuous models considered input and calculated models nicely agree. The use of the extended line set improves the fit (compare σ (cf. Equation (21)) in Table II). For delta-type models the maxima of the calculated distributions coincide well with the position T_δ of the delta models. The FWHM

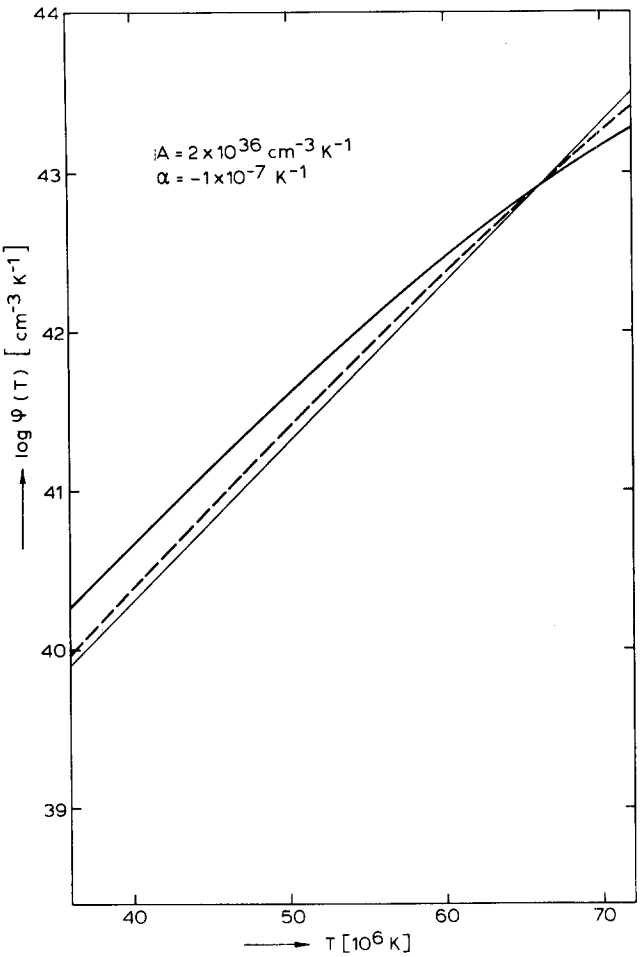

Fig. 4. Comparison of assumed (thin line) and calculated (heavy or dashed line) models. Heavy line indicates calculations with PMM line set, dashed line corresponds to calculations with extended line set.

values in Figures 5 and 6 and Table II indicate the resolution level that can be obtained with the line emission functions as given in Figure 1. It can be seen that these FWHM values are small for temperatures lower than 20×10^6 K, increasing rapidly for higher temperatures. The use of the extended line set improves the fit significantly (compare FWHM in Table II). For mixed models, visual inspection shows that calculated models are in qualitative agreement with the input models. Figures 7 and 8 clearly show that in many different situations the presence of quasi-isothermal regions embedded in a continuous temperature distribution can be resolved on a scale determined by the width of the line emission function used.

We should stress once more that, besides the method itself, the only *a priori* assumption used in the model calculations is, that the zero-approximation is chosen constant in all cases.

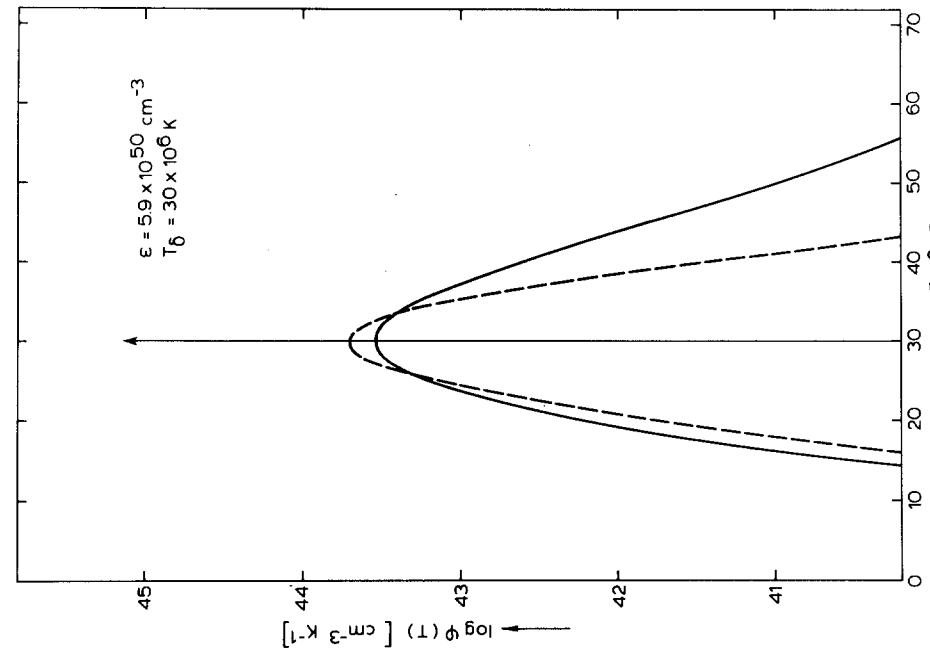

Fig. 6. For description see Figures 4 and 5.

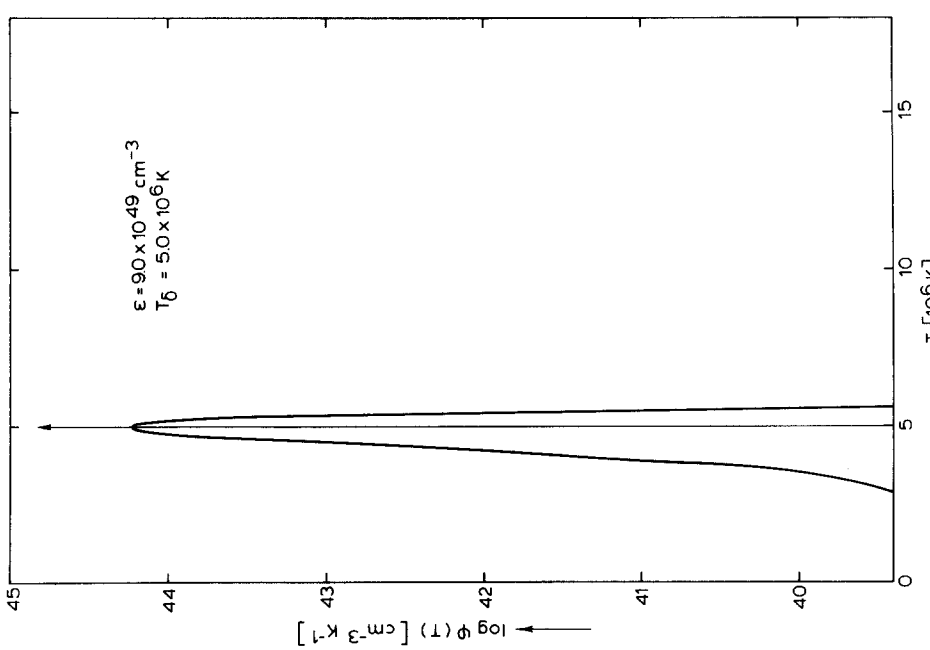

Fig. 5. For description see previous figure. The assumed model is isothermal with temperature T_δ denoted by the arrow.

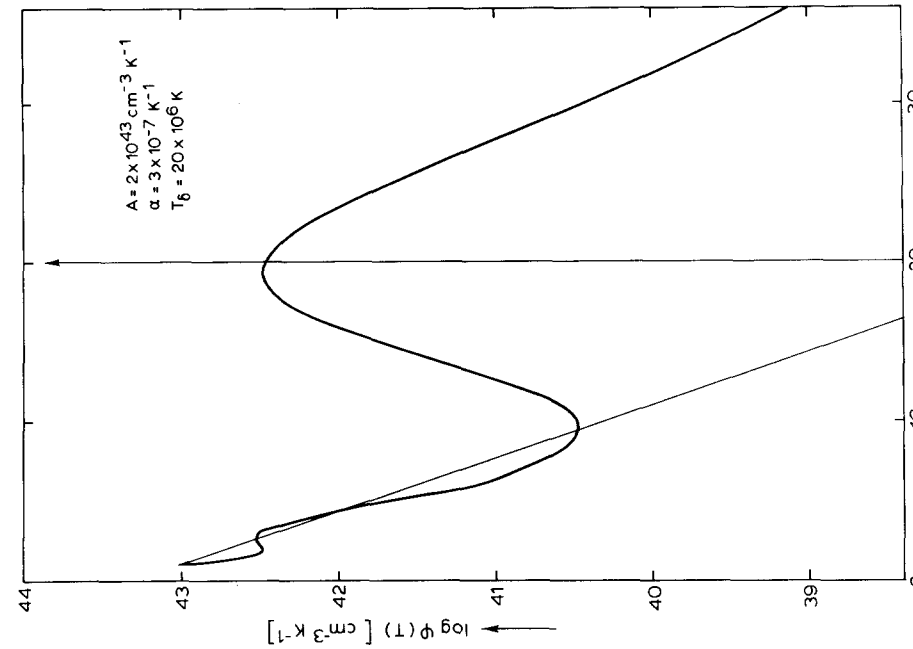

Fig. 8. For description see previous Figure.

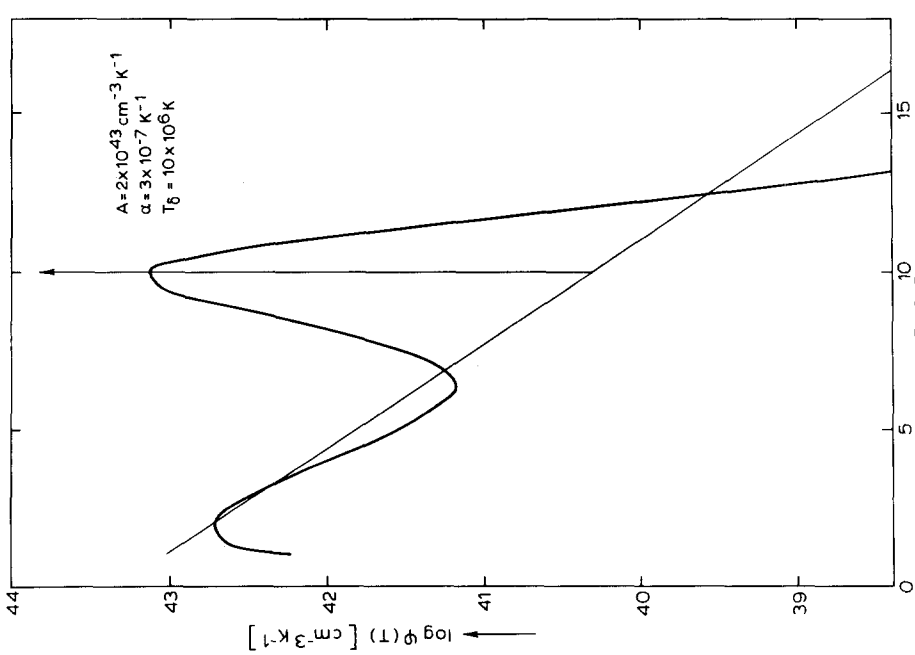

Fig. 7. Comparison of calculated (heavy line) with assumed (thin line) mixed model (continuous + δ-type).

TABLE II

The fit of calculated to input models.

Continuous models of the type $\phi_g(T) = A \times 10^{-\alpha T}$ ($cm^{-3}\,K^{-1}$)

Input model parameters			Calculations based on PMM line set			Calculations based on extended line set		
A ($10^{43}\,cm^{-3}\,K^{-1}$)	α ($10^{-7}\,K^{-1}$)	ε_g ($10^{48}\,cm^{-3}$)	σ (10^{-2})	χ^2	$\varepsilon_c/\varepsilon_g$	σ (10^{-3})	χ^2	$\varepsilon_c/\varepsilon_g$
2	5	5.49	3.06	5.06^{-5}	0.69	1.55	2.93^{-5}	0.96
2	3	14.5	3.28	1.91^{-3}	0.79	1.61	2.10^{-4}	0.98
2	1	69.0	3.47	8.15^{-2}	0.93	5.30	4.11^{-3}	1.00
2.0^{-7}	−1	109[a]	7.14	3.04	0.96	8.66	0.237	0.99

Delta-type isothermal models

Input model parameters		Calculations based on PMM line set			Calculations based on extended line set		
T_δ (10^6 K)	ε_g ($10^{49}\,cm^{-3}$)	T_m (10^6 K)	FWHM (10^6 K)	$\varepsilon_c/\varepsilon_g$	T_m (10^6 K)	FWHM (10^6 K)	$\varepsilon_c/\varepsilon_g$
2	3	2.0	<0.5	1.16	2.0	<0.5	1.16
5	9	5.0	<0.5	1.02	5.0	<0.5	1.02
7	13	7.0	0.5	1.00	7.0	<0.5	1.00
10	19	9.9	1.1	0.99	10.0	0.8	0.99
15	29	14.8	3.1	0.96	15.0	2.2	0.98
20	39	19.6	5.7	0.98	20.0	3.4	0.98
30	59	30.0	10.4	0.98	30.0	7.2	0.98
50	99	55.0	39.0	1.00	51.0	18.4	0.98

[a] Emission measure calculated inside the temperature interval $1\text{–}71 \times 10^6$ K.

N.B.: 5.06^{-5} means 5.06×10^{-5}, etc.

To be sure about the results of the iterative method, we have performed tests of the stability of the method. Using two input models, one continuous ($\phi_g(T) = 2 \times 10^{43} \times 10^{-3 \times 10^{-7} T}$), the other a delta-type one at temperature $T_\delta = 15 \times 10^6$ K, we calculated the full set of 14 expected line fluxes F_{ig} using Equation (20), after which we perturbed these fluxes randomly with amplitudes of 20, 30, and 50%. As a result of the perturbations we have obtained 14 fluxes F_{ip}. (For future use we define an input perturbation factor X_i as $X_i = F_{ip}/F_{ig}$). We then have used the perturbed fluxes for calculations of 'perturbed models'. For each family (corresponding to a given perturbation amplitude) of such models, presented in Figures 9 to 11 we have derived some mean characteristics and their standard deviations. We have put the results in Table III and in Figures 9, 10, and 11. The numbers in the columns of Table III headed by a given parameter are the arithmetic mean values obtained from 10 different calculations performed with a given perturbation amplitude. The columns marked 'dev' contain the values of the standard deviation in % of the corresponding

TABLE III
Analysis of iterative method stability

Amplitude input perturb. (%)	Continuous model $\phi_g(T) = 2\times10^{43}\times10^{-3\times10^{-7}T}$ cm^{-3} K^{-1}; $\varepsilon_g = 1.45\times10^{49}$ cm^{-3}											
	PMM line set						Extended line set					
	χ^2	dev. (%)	σ	dev. (%)	$\varepsilon_c/\varepsilon_g$	dev. (%)	χ^2	dev. (%)	σ	dev. (%)	$\varepsilon_c/\varepsilon_g$	dev. (%)
0	1.91^{-3}	–	3.28^{-2}	–	0.79	–	2.10^{-4}	–	1.61^{-3}	–	0.97	–
20	0.203	89	3.79^{-2}	51	0.88	33	0.482	160	2.31^{-2}	54	1.10	26
30	0.675	112	6.31^{-2}	66	0.94	38	0.652	76	3.00^{-2}	99	1.00	22
50	7.53	97	8.23^{-2}	70	0.90	53	2.36	56	0.202	60	1.78	55

Input pert. %	Delta-type model $T_\delta = 15\times10^6$ K; $\varepsilon_g = 2.9\times10^{50}$ cm^{-3}															
	PMM line set								Extended line set							
	χ^2	dev. (%)	T_m (10^6 K)	dev. (%)	FWHM (10^6 K)	dev. (%)	$\varepsilon_c/\varepsilon_g$	dev. (%)	χ^2	dev. (%)	T_m (10^6 K)	dev. (%)	FWHM (10^6 K)	dev. (%)	$\varepsilon_c/\varepsilon_g$	dev. (%)
0	2.24	–	14.8	–	3.1	–	0.98	–	1.79	–	15.0	–	2.2	–	0.99	–
20	27.6	82	14.7	2	3.44	20	0.95	4	31.0	37	14.96	1	2.15	11	1.00	4
30	64.9	34	14.8	2	3.10	23	1.00	6	87.7	37	14.91	1	1.91	22	0.98	6
50	182	61	14.7	4	3.42	26	0.98	7	287	43	14.60	3	2.10	23	0.96	9

N.B.: 1.91^{-3} means 1.91×10^{-3}, etc.

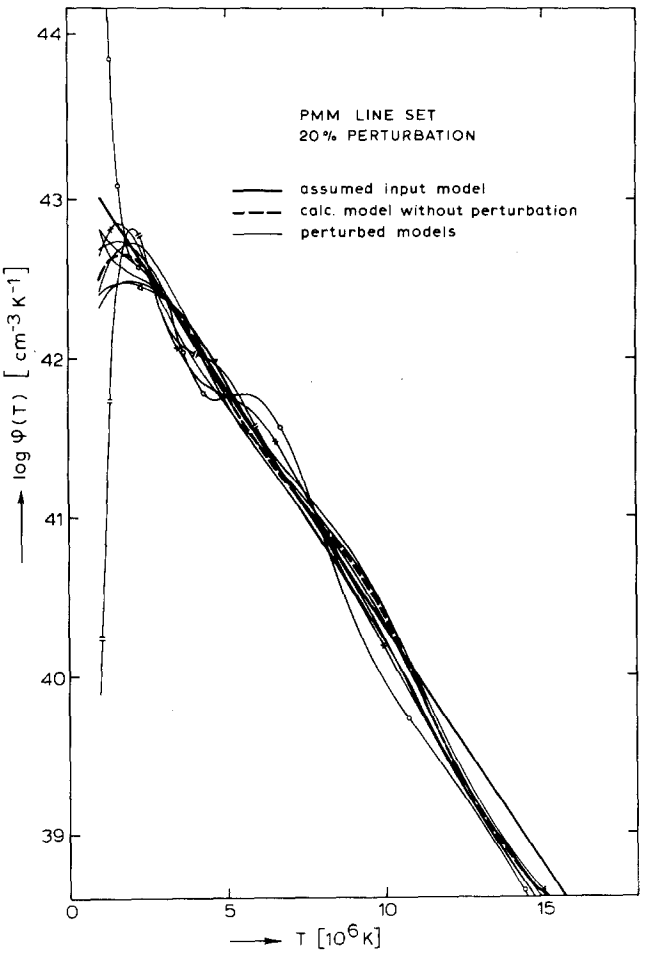

Fig. 9. Stability test of the iterative method. Each model plotted was calculated using the perturbed line fluxes (of the PMM line set). The amplitude of the random perturbation was taken equal to 20%. The unperturbed fluxes were calculated using the model $\phi(T) = 2 \times 10^{43}\, 10^{-3 \times 10^{-7} T}$ (cm^{-3} K^{-1}).

mean value. We have done two types of perturbation analysis, using model calculations both for the PMM set and the extended set of basic lines. The results of the stability analysis performed show that even 20% perturbations in the line fluxes are not followed by large disturbances in the calculated models. This result, valid for the PMM and the extended set extends the limits of the multitemperature analysis given by Craig and Brown (1976b) and Craig (1977).

It was found that the values of σ and χ^2 are not significantly correlated, but in most cases minimal χ^2 and minimal σ occur in the same iterations step. For large perturbations (30 and 50%) we have found some cases where the minimal χ^2 occurs before the minimal σ in the iteration process. But even in these cases the rise of χ^2

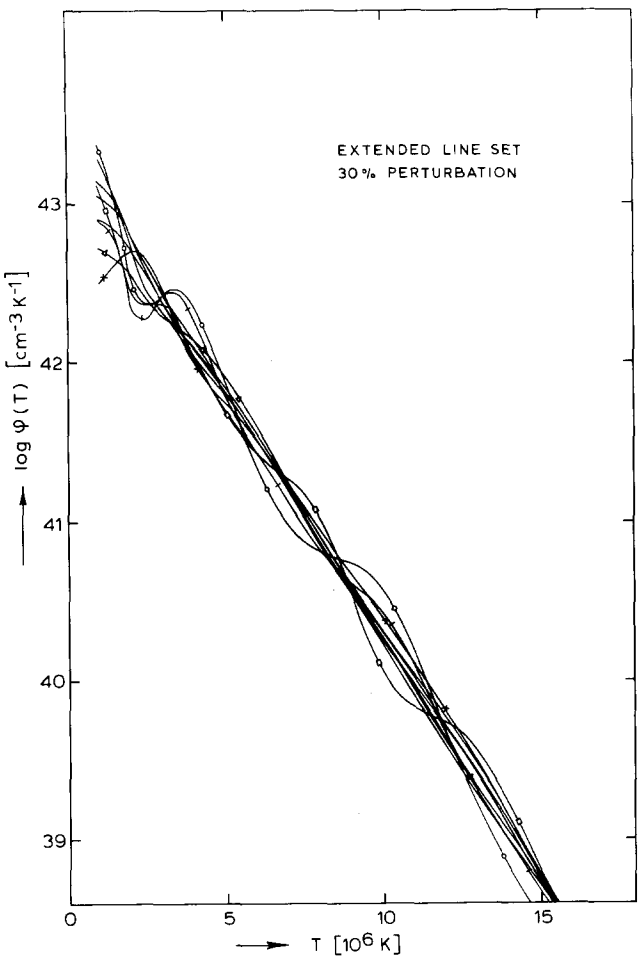

Fig. 10. For description see Figure 9. In this case the amplitude of the random perturbation in the line fluxes (of the extended line set) was assumed to be 30%. The same model $\phi(T)$ as in the previous case was used.

after the minimum was insignificant. For the largest perturbation (50%) in the continuous case, the minimal χ^2 occurs sometimes at the beginning of the iteration process (after 10–30 steps) and then χ^2 grows. In such cases the method is divergent.

The performed stability analysis indicates that the proposed method of DEM model calculations is sufficiently stable to be used in the analysis of X-ray line fluxes, when the fluxes are known with an accuracy better than 20% (the expected XRP accuracy is better). In the model calculations, besides the model itself, we can calculate the ratios of the observed input line flux to the calculated line flux (cf. Equation (13)), i.e. F_i/F_{ic}. In the case of the 'perturbed' calculations $F_i = F_{ip}$, so after the model calculations we can have $F_{ip}/F_{ic} = Y_i$ values also. We will call these ratios *detected* perturbations. Comparing these detected perturbations Y_i with the input

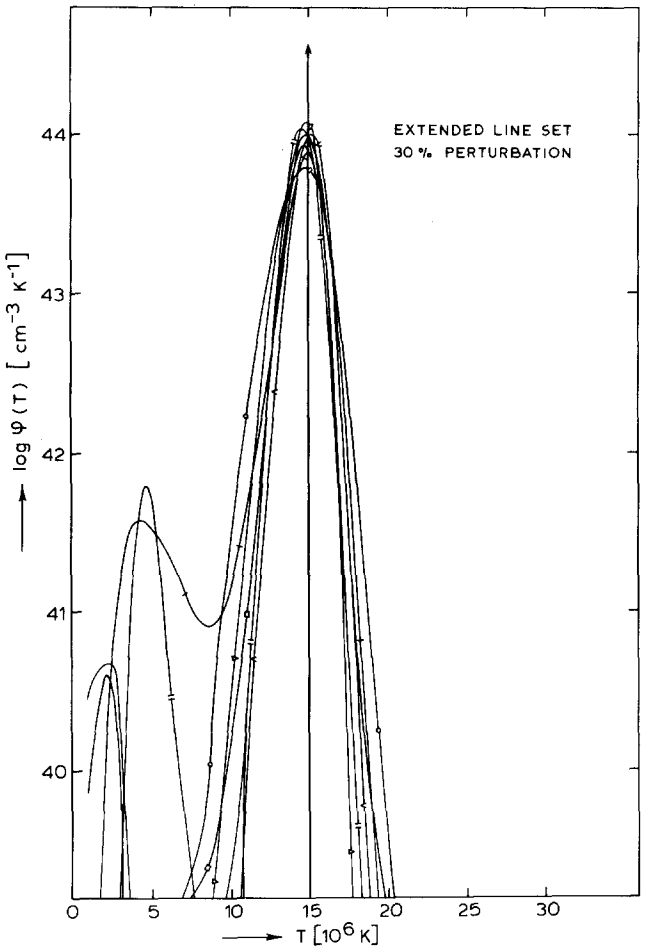

Fig. 11. For description see Figure 9. The random perturbation amplitude of the line fluxes (extended line set) was assumed to be 30%. The unperturbed line fluxes were calculated using a delta-type model with temperature $T_\delta = 15 \times 10^6$ K.

perturbations X_i (defined previously), we have found that for most lines used, the input and detected perturbations are highly correlated. In Table IV we present the results of the correlation analysis for each line separately. In deriving the correlation properties we have used the extended set of lines, taking the input and output factors from the stability calculations. In Table IV we give the correlation coefficients r, and the parameters defining the regression line. For both cases we see that the regression line crosses the point (1, 1) within an accuracy of some percent (see $a + b$ row). This means that if the input perturbation factor is 1 (no perturbation) then the expected detected perturbation is 1 too. The results of the correlation analysis show that for all the lines used (except lines No. 1, 13, and 14, for the continuous case, and line 1, for delta-type models) the input and output perturbation factors are well correlated. This fact allows us to track possible errors in the instrument calibration, the element

TABLE IV

Correlation between input perturbation ($X_i = F_{ip}/F_{ig}$) and detected perturbation ($Y_i = F_{ip}/F_{ic}$)

Continuous model

Line No.	1	2	3	4	5	6	7	8	9	10	11	12	13	14
r	−0.33	0.79	0.87	0.85	0.80	0.80	0.90	0.90	0.87	0.85	0.73	0.76	0.50	0.30
a	−0.27	0.68	0.69	0.81	0.50	0.87	0.97	0.60	0.66	0.76	0.50	0.54	0.14	0.06
b	1.19	0.35	0.33	0.22	0.51	0.13	0.10	0.39	0.32	0.22	0.48	0.48	0.87	0.93
$a+b$	0.92	1.03	1.02	1.03	1.01	1.00	1.07	0.99	0.98	0.98	0.98	1.02	1.01	0.99

Delta-type model

Line No.	1	2	3	4	5	6	7	8	9	10	11	12	13	14
r	0.59	0.80	0.71	0.95	0.92	0.97	0.95	0.97	0.91	0.93	0.97	0.96	0.95	0.89
a	0.25	0.64	0.62	0.89	0.75	0.97	1.09	0.86	1.08	0.77	0.83	0.74	0.88	0.70
b	0.64	0.39	0.40	0.15	0.31	0.06	−0.06	0.12	−0.10	0.17	0.14	0.18	0.10	0.21
$a+b$	0.89	1.03	1.02	1.04	1.06	1.03	1.03	0.98	0.98	0.94	0.97	0.92	0.98	0.91

N.B.: r – correlation coefficient.
a, b – regression line coefficients ($\hat{Y} = aX + b$).

abundances or the emission function approximations, viz., if after many real model calculations it turns out that the detected perturbation factors systematically differ from unity. It will be hard to decide what kind of error causes the difference. We have performed calculations which indicate that when inappropriate approximations for the emission functions are used, for instance, systematically 20% too low, we can not reproduce the measured line fluxes in both H- and He-like ions in the model calculations. It turns out that in this case the calculated He-like ion line intensities are about 10% too low, while the H-like line intensities are about 10% too high. So, if a systematic difference exists between the fit of the H- and He-like ion line intensities, it may indicate an error in the approximation used for the calculation of the H/He emission functions.

The results of the use of inappropriate element abundances are shown in Table V. In this table we present the effects caused by applying a perturbation of -20% to the abundance of one element on the value of the detected perturbations in all lines. We observe typically that the detected perturbations in the lines belonging to the perturbed element agree qualitatively with the inserted perturbation (the same sign, approximately half the amplitude) while in 2–3 neighbouring lines from other elements the reverse effect, i.e. enhancement of the intensity can be seen. This effect, as in the previous case, is weak for the 'boundary' Fe and O lines (Nos. 1, 2, 13, and 14). If other sources of errors can be assumed to be unimportant, the pattern observed in Table V can be used to improve the relative abundances of the elements used in the model calculations. Unfortunately, however, H- and He-like resonance lines, originating from the same element fall within the same channel of the FCS. Consequently errors in the relative calibration of the FCS sensitivity in different channels will result in values of the detected perturbation that are very similar to those caused by errors in the relative abundances. The problem of the separation of the abundance and calibration errors seems not easy to solve. We should mention that this problem is common to any method of line flux analysis, based on the considered PMM or Extended line sets. We hope that the fact, that the wavelength bands corresponding to each FCS channel overlap a little, can help in eliminating the uncertainties in the relative spectrometer calibration. Measurements of the continuum radiation level can also be very helpful in this context.

Notwithstanding the different sources of errors, which probably will be small, the following procedure can be developed, which allows the study of a possible abundance differentiation in the coronal plasma.

From the measured data (line fluxes in the extended set of lines) we choose a statistically significant set (hereafter reference set) corresponding to some preselected type of plasma. If, as a result of the model calculations performed for the reference set the detected perturbation factors differ systematically from unity, we can formally 'recalibrate' the instrument or abundances or emission function approximations by applying to the measured line fluxes the multiplying correction factors in accordance to the regression line parameters given in Table IV, so as to provide a statistically exact agreement between the observed and modelled line

TABLE V

Perturbations in element abundances as detected in model calculations

Line No.		1	2	3	4	5	6	7	8	9	10	11	12	13	14
Fe	I	−20	−20												
	D	0	−9	+11	−1	−2	0	−1	0	+1	0	0	0	0	0
Ca	I			−20	−20										
	D	0	+10	−11	−14	+9	+2	+7	0	0	−1	−1	+1	0	0
S	I					−20	−20								
	D	0	+1	+4	+9	−13	−15	+9	+3	+5	+1	+1	0	0	0
Si	I							−20	−20						
	D	0	−1	0	+6	+2	+8	−13	−15	+9	+3	+2	0	0	0
Mg	I									−20	−20				
	D	0	+1	0	0	−3	+7	+2	+9	−12	−14	+8	+2	+1	0
Ne	I											−20	−20		
	D	0	−1	+1	0	0	−1	0	+2	−3	+11	−8	−7	+4	0
O	I													−20	−20
	D	0	0	+1	0	−1	0	+1	0	+1	−1	−3	+8	−4	0

N.B.: I – input perturbation (%) of the element abundance.
D – detected perturbation (%) of the line intensity.

fluxes for the reference data set. We can use the derived correction factors to correct the line fluxes measured in other data sets. If for such a corrected data set, significant differences between corrected and modelled fluxes exist, these should be interpreted as a result of differences between the element abundances in the reference and the given type of plasma. Using such a procedure we hope to measure differences in the element abundances with an accuracy of a few per cent (physical processes which could cause differences in element abundances even within one active region are mentioned by Tworskowski (1975)).

6. Conclusions

We have performed a detailed analysis of a new iterative method for calculating the temperature distribution of the emission measure from X-ray line flux measurements. The method is designed to be used in the the interpretation of spectra to be measured by the X-ray Polychromator on board the Solar Maximum Mission. After various tests of the method, we have established its high usefulness, generality, stability, and ability to fit different kinds of simulated active region models. It turns out that the results of a multitemperature analysis may be helpful for the final improvement of relative spectrometer calibration. The possibility of deriving relative element abundances has been discussed. The method presented can be used for multitemperature analysis of both non-flaring and flaring active region plasmas under conditions of quasi-stationarity. The results of the paper extend the limits of the multitemperature analysis of line spectra as given by Craig and Brown (1967a, b).

We have not analysed existing X-ray line flux measurements. Such attempts were made already in the papers of Sylwester (1977, 1980) (analysis of flare spectra measured and reduced by Walker (1974a)), and in the paper of Jakimiec *et al.* (1980) (analysis of narrow band, Ross-filter spectroheliograms from OSO-7, corresponding to a decaying post-flare loop). The proposed method of analysis can probably be used as well in the analysis of center-to-limb optical darkening, and in the analysis of hard X-ray data.

Acknowledgements

The authors wish to thank Dr J. C. Brown for reading the manuscript and helpful comments.

One of us (J. Sylwester) thanks the Dutch Ministry of Education for financial support during his six month stay in Utrecht.

References

Acton, L. W. *et al.*: 1980, *Solar Phys.* **65**, 53.
Batstone, R. M., Evans, K., Parkinson, J. H., and Pounds, K. A.: 1970, *Solar Phys.* **13**, 389.
Chambe, G.: 1971, *Astron. Astrophys.* **12**, 210.
Craig, I. J. D.: 1975, in S. R. Kane (ed.), 'Solar Gamma-, X-, and EUV Radiation', *IAU Symp.* **68**, 187.

Craig, I. J. D.: 1977, *Astron. Astrophys.* **61**, 575.
Craig, I.J.D. and Brown, J.C.: 1976a, *Nature*, **264**, 341.
Craig, I.J.D. and Brown, J.C.: 1976b, *Astron. Astrophys.* **49**, 239.
Dere, K. P., Horan, D. M., and Kreplin, R. W.: 1974, *Solar Phys.* **36**, 459.
Herring, J. R. H. and Craig, I. J. D.: 1973, *Solar Phys.* **28**, 169.
Horan, D. M.: 1971, *Solar Phys.* **21**, 188.
Horan, D. M., Dere, K. P., and Kreplin, R. W.: 1974, *Space Res.* **XIV**, 441.
Jakimiec, J., Krutov, V. V., Mandelstam, S. L., Sylwester, B., Sylwester, J., and Zhitnik, I. A.: 1974, *Space Res.* **XIV**, 425.
Jakimiec, J., Neupert, W. M., Sylwester, B., and Sylwester, J.: 1980, to be published in *Proceedings of IX Consultation on Solar Physics*, Wrocław, Poland, 1978.
Jefferies, J. T., Orral, G. Q., and Zirker, J. B.: 1972, *Solar Phys.* **22**, 307.
Jordan, C.: 1976, in S. R. Kane (ed.), 'Solar Gamma-, X-, and EUV Radiation', *IAU Symp.* **68**, 109.
Kahler, S. W., Meekins, J. F., Kreplin, R. W., and Bowyer, S. C.: 1970, *Astrophys. J.* **162**, 293.
Korneev, V. V., Krutov, V. V., Mandelstam, S. L., Urnov, A. M., Zhitnik, I. A., Kononov, A. Ya., Sylwester, B., and Sylwester, J.: 1979, *Solar Phys.* **63**, 319.
Landini, M. and Monsignori Fossi, B. C.: 1979, *Astron. Astrophys.* **72**, 171.
Landini, M., Monsignori Fossi, B. C., and Pallavicini, R.: 1972, *Solar Phys.* **27**, 164.
Lampton, M., Morgan, B., and Bowyer, S. C.: 1976, *Astrophys. J.* **208**, 177.
Meekins, J. F.: 1973, Thesis, Catholic University, Washington.
Mewe, R. and Schrijver, J.: 1978, *Astron. Astrophys.* **65**, 99.
Mewe, R., Schrijver, J., and Sylwester, J.: 1980a, *Astron. Astrophys.* **87**, 261.
Mewe, R., Schrijver, J., and Sylwester, J.: 1980b, *Astron. Astrophys. Suppl. Ser.* **40**, 323.
Parkinson, J. H.: 1975a, *Solar Phys.* **42**, 183.
Parkinson, J. H.: 1975b, in S. R. Kane (ed.), 'Solar Gamma-, X-, and EUV Radiation', *IAU Symp.* **68**, 45.
Phillips, K. J. H.: 1975, *Astrophys. J.* **199**, 247.
Rapley, C.: 1977, private communication.
Rust, B. W. and Burrus, W. R.: 1972, *Modern Analytic and Computational Methods in Science and Mathematics*, Elsevier, New York.
Sylwester, J.: 1977, Thesis, Wrocław University, Poland.
Sylwester, J.: 1980, to be published in *Proceedings of IX Consultation on Solar Physics*, 1978, Wrocław, Poland.
Sylwester, J., Mewe, R., and Schrijver, J.: 1980, *Astron. Astrophys. Suppl. Ser.* **40**, 335.
Tworkowski, A. S.: 1975, *Astrophys. Letters* **17**, 27.
Vainshtein, L. A. and Safronova, U. I.: 1978, *Atomic Data and Nuclear Data Tables* **21**, 49.
Walker, A. B. C., Jr.: 1972, *Space Sci. Rev.* **13**, 672.
Walker, A. B. C., Jr.: 1975, in S. R. Kane (ed.), 'Solar Gamma-, X-, and EUV Radiation', 73.
Walker, A. B. C., Jr., Rugge, H. R., and Weiss, K.: 1974a, *Astrophys. J.* **188**, 423.
Walker, A. B. C., Jr., Rugge, H. R., and Weiss, K.: 1974b, *Astrophys. J.* **192**, 169.
Walker, A. B. C., Jr., Rugge, H. R., and Weiss, K.: 1974c, *Astrophys. J.* **194**, 471.
Withbroe, G. L.: 1975, *Solar Phys.* **45**, 301.